


Article

Investigation into Viscoelastic Properties of Fiber-Reinforced Asphalt Composite Concrete Based on the Burgers Model

Chunshui Huang ^{1,2,3}, Danying Gao ², Tong Meng ³ and Changde Yang ^{4,*} 

¹ School of Civil Engineering, Xuchang University, Xuchang 461000, China

² School of Civil Engineering, Zhengzhou University, Zhengzhou 450001, China

³ School of Civil Engineering, North China University of Water Resources and Electric Power, Zhengzhou 450046, China

⁴ School of Mines, China University of Mining and Technology, Xuzhou 221116, China

* Correspondence: ycd@cumt.edu.cn

Abstract: Asphalt composite concrete pavement is one of the common pavement forms in China. However, due to the influence of design, materials, construction quality, and other aspects, asphalt composite concrete pavement develops various degrees of cracks after being put into use, which affects the service performance and life of asphalt pavement. The Burgers model is used to examine the effects of fiber-volume-fraction and length–diameter-ratio on the viscoelastic mechanical behavior model parameters and viscoelastic properties of asphalt composite concrete through the bend test for creep of polyester fiber asphalt composite concrete beam. The findings indicate that the fiber’s ability to control asphalt composite concrete bending creep deformation increases initially and subsequently diminishes as fiber-volume-fraction and length–diameter-ratio increase. Fiber-volume-fraction and length–diameter-ratio effects can be fully reflected by fiber amount characteristics. A viscoelastic mechanical behavior model of fiber-reinforced asphalt composite concrete is developed on this foundation while taking into account the influence of fiber amount characteristic factors. Theoretical study and practical research indicate that the ideal fiber volume ratio of polyester fiber asphalt composite concrete is 0.35 percent, the ideal length-to-diameter ratio is 324, and the ideal fiber amount characteristic parameter is 1.13. The test results can provide a certain reference value for the improvement of the long-term durability of fiber asphalt composite concrete pavement of road engineering.

Keywords: asphalt composite concrete; fiber-reinforced; viscoelastic properties; bend tests for creep; Burgers model



Citation: Huang, C.; Gao, D.; Meng, T.; Yang, C. Investigation into Viscoelastic Properties of Fiber-Reinforced Asphalt Composite Concrete Based on the Burgers Model. *Buildings* **2023**, *13*, 449. <https://doi.org/10.3390/buildings13020449>

Academic Editor: Pengfei Liu

Received: 4 January 2023

Revised: 26 January 2023

Accepted: 3 February 2023

Published: 6 February 2023



Copyright: © 2023 by the authors. Licensee MDPI, Basel, Switzerland. This article is an open access article distributed under the terms and conditions of the Creative Commons Attribution (CC BY) license (<https://creativecommons.org/licenses/by/4.0/>).

1. Introduction

China has the most expressways in the world, with a total mileage of 150,000 km in 2020, according to statistics from the Ministry of Transport [1–3]. The evolution process of China’s expressway mileage from 2010 to 2020 is shown in Figure 1. As asphalt composite concrete pavement has the advantages of a short construction period, smoothness, comfort, low noise, and convenient maintenance. Asphalt composite concrete pavement structure accounts for more than 90 percent of the expressway that has been opened to traffic in China. Therefore, a large amount of asphalt composite concrete material is required every year in China [4–6]. Asphalt composite concrete pavement is the main part of the expressway, therefore, its characteristics have important impacts on the safety, comfort, and durability during the expressway service process [7,8].

A typical viscoelastic composite material, asphalt composite concrete is a three-phase system made up of an asphalt binder, a mineral mixture, and air. In order to investigate the effects of temperature, loading stress level, modifiers, additives, etc., on the viscoelastic properties of asphalt composite concrete, various viscoelastic mechanical behavior models are currently combined with viscoelastic basic elements such as dampers and springs [9–14].

These tests are based on the uniaxial compression creep test, triaxial compression creep test, and small beam bend test for creep [15–17]. Numerous constitutive models based on viscoelastic mechanics have been proposed in order to investigate the viscoelastic deformation properties of asphalt composite concrete, most notably the simple Kelvin model and Maxwell model, the three-element Vendepoel model and Lethersich model, the four-element Burgers model, and the generalized Kelvin model and Maxwell model with more elements [18–21]. Additionally, Gao et al. [19] proposed a five-element model with eight parameters, which can better describe the creep deformation characteristics of plain asphalt mixtures and fiber-reinforced asphalt mixtures. The fitting results obtained from the model are consistent with the data from measurements, and the rheological time it predicts is accurate. To characterize the creep deformation trend of rubber particles and diatomite asphalt mixture, Liang et al. [20] proposed a modified Burgers model. This model is obviously superior to the Burgers model, and its fitting results at the later stages of creep deformation are more in line with actual experimental findings. According to Ni [22], the mechanical properties of asphalt composite concrete are closely related to loading time and ambient temperature, and the effects of loading time and ambient temperature should be considered concurrently in the mechanical analysis of asphalt pavement structure; the structural mechanical response of asphalt pavement with multi-layer viscoelastic properties can be calculated using the elastic viscoelastic correspondence principle.

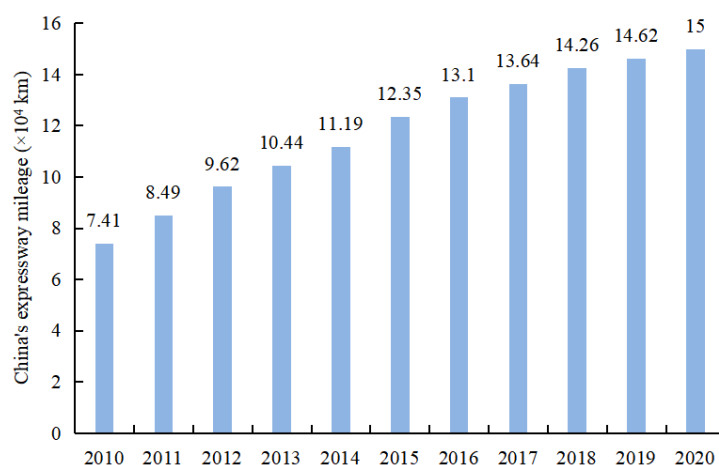


Figure 1. Evolution process of China's expressway mileage from 2010 to 2020.

Fiber is added to asphalt composite concrete to considerably increase the overall mechanical performance and durability of asphalt composite concrete pavement, hence extending its useful life and addressing the issue of early damage [23]. The research on the viscoelastic properties of fiber-reinforced asphalt composite concrete has drawn increasing attention worldwide due to the fact that the inclusion of fiber can greatly improve the road performance of asphalt composite concrete [24–27]. Through the compression creep test of polyester fiber-reinforced asphalt composite concrete, Guo and Guo [28] investigated the impact of fiber length on the viscoelastic performance of asphalt composite concrete in the creep loading stage under different fiber amounts. They then established a viscoelastic mechanical behavior model of fiber-reinforced asphalt composite concrete taking the influence of fiber amount into consideration. Through a pull-out test, Liang [29] examined the impact of fiber length on the performance of asphalt composite concrete. Rheological testing and microscopic examination of the fiber asphalt matrix material were carried out by Chen and Lin [30]. The findings demonstrate that the distribution of fiber in asphalt is random in three dimensions, which has a positive influence on bonding and greatly raises the viscosity ratio between fiber-reinforced asphalt composite concrete and regular asphalt composite concrete. Through the Marshall test, static triaxial test, and dynamic triaxial test, Bueno et al. [31] investigated the effects of fiber amount and length on the mechanical properties of fiber-reinforced cold-mixed asphalt composite concrete.

According to the findings, the fiber output is between 0.10 and 0.25 percent, and the 40 mm fiber exhibits good reinforcement properties. Chen [32] analyzed the influence of the fiber on the pavement performance, expatiated the strengthening mechanism of the fiber asphalt composite concrete pavement with the theory of composite materials and the interfacial chemistry through the tests of the six fibers and three gradations, the asphalt mixture of different combination. Zhou [33] studied the fatigue damage behavior of asphalt mixture and the fatigue failure of asphalt pavement and predicted the fatigue life of AC overlay on existing PCC pavement based on the theory and method of fatigue damage mechanics. Chen [34] paved the corn stalk fiber and basalt fiber SMA-13 mixture indoor test road, carried out the production mix ratio design and summarized the corn stalk fiber and basalt fiber asphalt mixture road construction technology. Then, based on the full-scale accelerated loading test, the rutting depth of the corn stalk fiber and basalt fiber SMA-13 surface layer structure and the lignin fiber SMA-13 surface layer structure were analyzed. The research results showed that the corn stalk fiber and basalt fiber SMA-13 surface layer structure has a longer service life [35–37]. Nevertheless, there are still a lot of issues in the current research that need to be resolved, including the effects of fiber aspect ratio on the parameters of the viscoelastic mechanical behavior model and the viscoelastic properties of asphalt composite concrete, as well as the effects of fiber-volume-fraction and aspect ratio on the parameters of the viscoelastic mechanical behavior model and the viscoelastic properties of asphalt composite concrete after unloading. How to apply a parameter to accurately depict the impact of fiber-volume-fraction and aspect ratio on the viscoelastic mechanical characteristics of asphalt composite concrete is another important consideration.

In this study, the ideal asphalt content was established using the conventional Marshall test method, and the tiny beam bend test for creeps was then conducted using the variables fiber volume percent V_f and length–diameter-ratio R_a . The effects of V_f and R_a on the parameters of the viscoelastic mechanical behavior model and the viscoelastic characteristics of asphalt composite concrete throughout the creep loading and unloading stages were carefully investigated using Burger’s model as a foundation. To fully portray the impact of V_f and R_a , fiber amount characteristic parameters λ_f were used. Last but not least, a viscoelastic mechanical behavior model of fiber-reinforced asphalt composite concrete was created and a viscoelastic analysis was performed.

2. Materials and Methods

2.1. Materials

No. 70 road petroleum asphalt is used in the tests, and its main physical performance indexes are shown in Table 1. The V_f of polyester fiber with R_a of 162, 486, and 649 is 0.35 percent. In addition, the V_f of polyester fiber with R_a of 324 are 0.17 percent, 0.35 percent, 0.52 percent, and 0.69 percent, respectively. After sieving, cleaning, and drying, the aggregate is mixed with limestone powder to form AC-13F median grading. Determine the optimum asphalt content of the base asphalt mixture and asphalt mixture with different V_f and R_a through the standard Marshall test method. The designed polyester fiber asphalt mixture is rolled into 300 mm × 300 mm × 50 mm (L × W × H) test pieces, then cut into 250 mm × 30 mm × 35 mm (L × W × H) small beam specimens, and conduct bend test for creeps on multi-functional material testing machine, and load with weights, as shown in Figure 2.

Table 1. Mainly physical performance indexes of No. 70 road petroleum asphalt.

Road Petroleum Asphalt	Penetration Ratio at 25 °C $P/0.1\text{ mm}$	Ductility at 25 °C D/cm	Softening Point SP/°C	Density $\rho_b/\text{g/cm}^3$
No. 70	75	≥100	44.3	1.00937

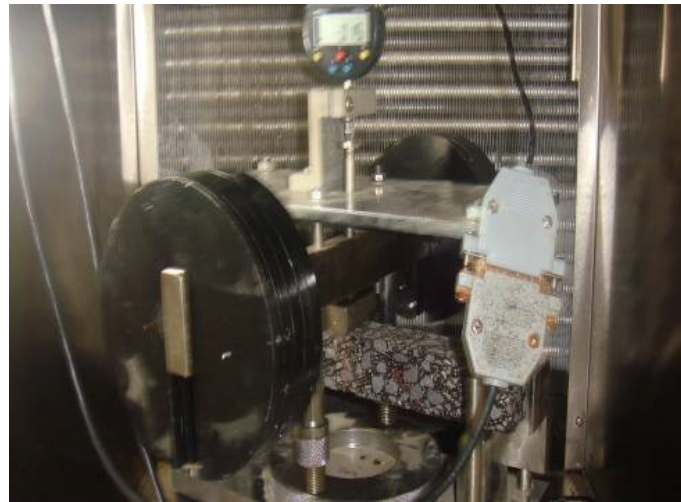


Figure 2. Small beam bend test for creeps.

Under identical circumstances, the creep load is 10 percent of the little beam's bending failure force. A total of eight groups of creep tests were carried out on three trabecular specimens repeated in each group. During the test, the dial indicator connected with the data acquisition system is used to collect the mid-span deflection of the small beam during the creep test, collect the data every one second and draw the mid-span deflection time relationship curve. When the beam specimen enters the accelerated creep stage, remove the load and continue to collect the mid-span deflection data of the beam within 30 min of unloading.

2.2. Method

The deformation process of viscoelastic materials changing with time mainly includes creep, stress relaxation, hysteresis, and strain rate sensitivity. In engineering, viscoelastic basic elements (springs and dampers) are often combined into different viscoelastic mechanical behavior models in different ways to describe their creep deformation characteristics. It is generally believed that the Burgers model can best reflect the creep and relaxation characteristics of asphalt composite concrete, so the Burgers model viscoelastic constitutive model is widely used in the field of road engineering [38–41]. The Burgers model is composed of two springs and two dampers. As shown in Figure 3, the Burgers model can better reflect the viscoelastic deformation characteristics of asphalt composite concrete materials.

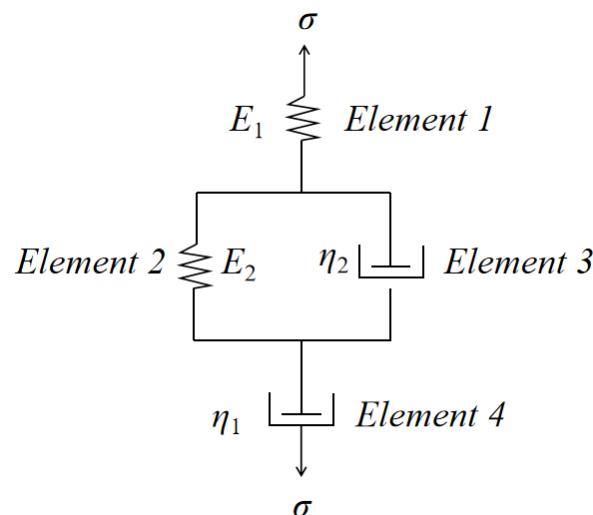


Figure 3. Burgers model.

Although the creep deformation of fiber-reinforced asphalt composite concrete with different V_f and R_a is different, the creep deformation time curve presents three stages of deceleration creep, constant velocity creep, and accelerated creep, and the creep deformation characteristics of asphalt composite concrete itself are not changed by adding fiber. As a result, a viscoelastic mechanical behavior model of fiber-reinforced asphalt composite concrete may be built based on the viscoelastic mechanical behavior model of regular asphalt composite concrete and take into account the influence of fiber on the model's characteristics. The viscoelastic creep equation for fiber-reinforced asphalt composite concrete, as shown in Figure 3, is as follows:

Loading stage:

$$\varepsilon = \sigma_0 \left(\frac{1}{E_1} + \frac{t}{\eta_1} + \frac{1 - e^{-t\tau}}{E_2} \right) \quad (1)$$

Unloading stage:

$$\varepsilon = \sigma_0 \left[\frac{t_0}{\eta_1} + \frac{(1 - e^{-t_0\tau})e^{-\tau(t-t_0)}}{E_2} \right] \quad (2)$$

where E_1 and η_1 represent, respectively, the elastic modulus of elastic element 1 and the viscosity of viscous element 4, taking into account the influence of fibers; and E_2 and η_2 represent, respectively, the elastic modulus of element 2 and the viscosity of element 3, taking into account the influence of fibers; $\tau = \frac{E_2}{\eta_2}$.

In the model of Equations (1) and (2), the more E_1 is greater, the more elastic deformation fiber-reinforced asphalt composite concrete can withstand. The amount of permanent deformation of fiber-reinforced asphalt composite concrete under the same weight and duration decreases with increasing value of η_1 . The slower the viscous deformation rises over time and the smaller the rutting depth of fiber-reinforced asphalt composite concrete pavement is related to relaxation time η_1/E_1 . The ability of fiber-reinforced asphalt composite concrete to withstand viscoelastic deformation is increased by increasing the delay time η_2/E_2 , which also slows the development of viscoelastic deformation over time.

The creep strain time data gathered in the test is imported using Origin 8.5 software's nonlinear fitting approach in accordance with the results of the creep test. By assuming the beginning values of the model parameters and altering the model parameters to make the theoretical calculation results of the model best fit the experimentally measured values, the parameters of the viscoelastic mechanical behavior model based on Equations (1) and (2) are established. The impacts of V_f and R_a on model parameters are examined in light of this. The creep equation and constitutive equation are used to perform the viscoelastic analysis of fiber-reinforced asphalt composite concrete. The constitutive equation of fiber-reinforced asphalt composite concrete is established by using the parameter λ_f as the parameter comprehensively reflecting the influence of V_f and R_a .

3. Results

3.1. Effects of V_f on the Parameters of Equation (1) Model

Equation (1) model is composed of the Maxwell model and Kelvin model in series. In this model, the elastic element E_1 produces instantaneous elastic deformation that can be recovered immediately after unloading. The resistance of fiber-reinforced asphalt composite concrete to elastic deformation increases with the value. The viscous element η_1 causes permanent deformation in the viscous flow that is irreversible after unloading. The permanent deformation caused by the same load at the same moment decreases as the value increases. The expansion of viscous deformation occurs more slowly and the depth of rutting in fiber-reinforced asphalt composite concrete pavement decreases with increasing relaxation time η_1/E_1 . Under the influence of E_2 , the deformation produced in the viscoelastic composite element η_2 and E_2 will recover gradually. The deformation of fiber-reinforced asphalt composite concrete material develops more slowly and is more resistant to deformation the longer the delay time η_2/E_2 . Table 2 displays the model parameters for Equation (1) for fiber-reinforced asphalt composite concrete with various

fiber-volume-fractions. It is clear that as the fiber-volume-fraction rises, E_1 first rises and then falls. The greatest value is attained when the fiber-volume-fraction is 0.35 percent. The elastic deformation resistance to the transient load of fiber-reinforced asphalt composite concrete is now very strong. Fiber can only improve the elasticity of asphalt composite concrete when the fiber volume percent is adequate, as evidenced by the fact that when the fiber-volume-fraction reaches 0.69 percent, the value of fiber-reinforced asphalt composite concrete E_1 is lower than that of matrix asphalt composite concrete. As the fiber-volume-fraction rises, the value of η_1 first rises and then falls. The greatest value, which is more than twice the value of the matrix asphalt composite concrete, is attained when the fiber-volume-fraction is 0.35 percent. The fiber-reinforced asphalt composite concrete's η_1 is smaller than the matrix asphalt composite concrete when the fiber-volume-fraction exceeds 0.69 percent.

Table 2. Equation (1) model parameters of asphalt composite concrete with different V_f .

$V_f/\%$	Parameters of Equation (1) Model				R^2	Relaxation Time $\eta_1/E_1/s$	Delay Time $\eta_2/E_2/s$
	E_1/MPa	E_2/MPa	$\eta_1/MPa \cdot s$	$\eta_2/MPa \cdot s$			
0	629	110	305,403	30,110	0.99912	485	274
0.17	726	144	530,628	43,517	0.99815	731	302
0.35	916	161	683,955	51,518	0.99540	746	320
0.52	793	148	501,683	46,680	0.99923	633	315
0.69	610	122	268,829	36,772	0.99913	315	301

As a result, fibers with the right volume fraction have positive effects on viscosity. The fiber exhibits a good viscosity-increasing effect at a volume percentage of 0.35 percent. At the moment, asphalt composite concrete with fiber reinforcement has a decent resistance to permanent deformation, and too much fiber lowers that resistance. The relaxation time η_1/E_1 and delay time η_2/E_2 of fiber-reinforced asphalt composite concrete first increase and then decrease with the increase in fiber-volume-fraction. When the fiber-volume-fraction is 0.35 percent, the relaxation time η_1/E_1 and delay time η_2/E_2 both reach the maximum value. As a result, adding the right quantity of fiber can increase asphalt composite concrete's resistance to rutting. The fiber has a better impact on the rutting resistance of asphalt composite concrete when the fiber volume ratio is 0.35 percent. E_1 , η_1 , η_1/E_1 , and η_2/E_2 increase first and then decrease with the increase in fiber-volume-fraction. When the fiber-volume-fraction is 0.35 percent, the maximum value appears. The best volume fraction of polyester fiber to play the best role in reinforcing is 0.35 percent at the moment because fiber-reinforced asphalt composite concrete has strong resistance to elastic deformation, viscous flow deformation, and rutting deformation.

3.2. Effects of V_f on the Parameters of Equation (2) Model

When the small beam bend test for the creep piece enters the accelerated creep stage, remove the load, collect the mid-span deflection of the beam test piece within 30 min after unloading, convert the deflection into strain, apply Origin 8.5 software to fit the test data and model parameters, and obtain the Equation (2) model parameters of asphalt composite concrete with different fiber-volume-fraction, as shown in Table 3. It can be seen that the same parameter values of the Equation (2) model and Equation (1) model are quite different. It is shown that the E_2 and η_2 value of Equation (1) model parameters greatly increases compared with the loading stage, and the delay time η_2/E_2 also increases, but η_1 significantly decreases.

This is so because the rapid creep stage of asphalt composite concrete is the creep failure stage. Dislocations and slides between the interior aggregates occur when asphalt composite concrete beams are bent, resulting in material damage and decreased performance. The mechanical model parameters obtained in the creep loading stage cannot be used to characterize the actual deformation characteristics of fiber-reinforced asphalt

composite concrete after unloading because the actual permanent deformation represented by the model parameters in the unloading stage is greater than the theoretical permanent deformation represented by the model parameters in the loading stage, and the rate of actual deformation recovery also becomes slow. Table 3 also shows that, in comparison to the creep loading stage, there is less of a correlation between the test data in the creep unloading stage and the model in Equation (2). This suggests that the Burgers model is more accurate at describing the viscoelastic deformation properties of asphalt composite concrete during the loading process.

Table 3. Equation (2) model parameters of asphalt composite concrete with different V_f .

$V_f/\%$	Parameters of Equation (2) Model			R^2	Delay Time $\eta_2/E_2/s$
	E_2/MPa	$\eta_1/MPa \cdot s$	$\eta_2/MPa \cdot s$		
0	343	251,554	109,199	0.98485	318
0.17	386	346,085	145,944	0.97533	378
0.35	406	399,097	170,332	0.99189	420
0.52	379	317,203	140,118	0.98291	370
0.69	345	184,746	119,707	0.98901	347

3.3. Effects of R_a on the Parameters of Equation (1) Model

Table 4 displays the model parameters that were produced using Equation (1) model and Origin 8.5 software fitting the test data of fiber-reinforced asphalt composite concrete creep loading stage with various fiber length–diameter-ratios. It is clear that as the fiber length-to-diameter ratio rises, the elastic modulus of elastic element E_1 in the model initially rises and then falls. The greatest value is attained at a fiber length–diameter-ratio of 324, and the fiber exhibits good elastic reinforcement. With an increase in the fiber length–diameter-ratio, the value of the model parameter η_1 first rises and subsequently falls. The greatest value is reached for a fiber length–diameter-ratio of 324. The value is raised by nearly two times when compared to the base asphalt composite concrete. The viscosity-increasing impact of the fiber is currently better, and fiber-reinforced asphalt composite concrete is more resistant to permanent deformation.

Table 4. Equation (1) model parameters of asphalt composite concrete with different R_a .

R_a	Parameters of Equation (1) Model				R^2	Relaxation Time $\eta_1/E_1/s$	Delay Time $\eta_2/E_2/s$
	E_1/MPa	E_2/MPa	$\eta_1/MPa \cdot s$	$\eta_2/MPa \cdot s$			
0	629	110	305,403	30,110	0.99912	486	274
162	823	144	541,533	43,359	0.99936	658	301
324	916	161	683,955	51,518	0.99540	747	320
486	705	139	364,537	43,405	0.99746	517	312
649	643	125	319,489	37,890	0.99118	497	303

With an increase in the fiber length–diameter-ratio, the relaxation time η_1/E_1 first rises and subsequently falls. The greatest value is seen when the fiber length–diameter-ratio reaches 324. The fiber-reinforced asphalt composite concrete currently offers greater resistance to rutting deformation. With an increase in the fiber length–diameter-ratio, the delay time η_2/E_2 first rises and subsequently falls. The highest delay time is reached at a fiber length–diameter-ratio of 324, and the fiber-reinforced asphalt composite concrete exhibits good resistance to long-term deformation. As can be observed, fiber-reinforced asphalt composite concrete is more resistant to elastic deformation, rutting deformation, and viscous flow deformation. The ideal fiber length-to-diameter ratio is 324.

3.4. Effects of R_a on the Parameters of Equation (2) Model

Table 5 displays the model parameters that were produced using Equation (2) model and Origin 8.5 software fitting the test data of fiber-reinforced asphalt composite concrete creep unloading stage with various fiber length–diameter-ratios. The values of the same model parameters have significantly altered in the two distinct stages of creep loading and creep unloading, as can be seen. The equation for the creep unloading stage (2), the actual permanent deformation of fiber-reinforced asphalt composite concrete with different fiber aspect ratios, as represented by the model parameters in the unloading stage, is greater than the theoretical permanent deformation, as represented by the model parameters in the creep loading stage. This is because the E_2 and η_2 values of the model parameters in the loading stage have a large increase, the delay time η_2/E_2 has a small increase, but η_1 has a large decrease. When compared to theoretical creep deformation, which is described by model parameters in the loading stage, actual creep deformation, as measured by unloading stage characteristics, recovers more slowly. At the unloading stage, there is less correlation between experimental data and the fiber-reinforced asphalt composite concrete model with various aspect ratios than there is at the loading stage.

Table 5. Equation (2) model parameters of asphalt composite concrete with different R_a .

R_a	Parameters of Equation (2) Model			R^2	Delay Time $\eta_2/E_2/s$
	E_2/MPa	$\eta_1/MPa \cdot s$	$\eta_2/MPa \cdot s$		
0	343	251,554	109,199	0.98485	318
162	369	310,862	141,021	0.98455	382
324	406	399,097	170,332	0.99189	420
486	364	292,954	139,592	0.99533	383
649	349	266,937	123,008	0.98254	352

3.5. Establishment of Constitutive Equation of Fiber-Reinforced Asphalt Composite Concrete

In summary, the length–diameter-ratio and fiber-volume-fraction have a significant impact on the viscoelastic characteristics of asphalt composite concrete. Using the models in Equations (1) and (2), the viscoelastic constitutive equations of fiber-reinforced asphalt composite concrete are developed for the creep loading stage and the unloading stage, respectively. The characteristic parameter of fiber amount $\lambda_f = V_f \times R_a$ is used to reflect the comprehensive influence of V_f and R_a . Equation (1) model parameters all have the change rule of first increasing and then decreasing with the increase in fiber amount characteristic parameters. The relationship between model parameters and fiber amount characteristic parameters of nonlinear fitting Equation (1) can be expressed as:

Loading stage:

$$E_1(\lambda_f) = 699.86 + 144.49\lambda_f - 37.60\lambda_f^2 \quad (3)$$

$$E_2(\lambda_f) = 124.74 + 29.09\lambda_f - 6.71\lambda_f^2 \quad (4)$$

$$\eta_1(\lambda_f) = 421224.53 + 164684.43\lambda_f - 44571.93\lambda_f^2 \quad (5)$$

$$\eta_2(\lambda_f) = 35795.38 + 12693.07\lambda_f - 2817.99\lambda_f^2 \quad (6)$$

By substituting Equations (3)–(6) into Equation (2), the creep equation of fiber-reinforced asphalt composite concrete characterized by the Burgers model considering the influence of λ_f can be obtained:

Loading stage:

$$\varepsilon(t, \lambda_f) = \sigma_0 \left[\frac{1}{E_1\lambda_f} + \frac{t}{\eta_1(\lambda_f)} + \frac{1 - e^{-t\tau}}{E_2(\lambda_f)} \right] \quad (7)$$

The derivative of Equation (7) with respect to time can be used to obtain the differential constitutive equation of fiber-reinforced asphalt composite concrete described by the Burgers model taking into account the influence of λ_f :

Loading stage:

$$d\varepsilon(t, \lambda_f)/dt = \dot{\varepsilon}(t, \lambda_f) = \sigma_0 \left[\frac{1}{\eta_1(\lambda_f)} + \frac{e^{-t\tau}}{\eta_2(\lambda_f)} \right] \quad (8)$$

Equation (2) model parameters all have the change rule of first increasing and then decreasing with λ_f . The relationship between the model parameters and λ_f of nonlinear fitting Equation (2) can be expressed as:

Unloading stage:

$$E_2(\lambda_f) = 343.43 + 103.25\lambda_f - 46.58\lambda_f^2 \quad (9)$$

$$\eta_1(\lambda_f) = 247449.9 + 275225.8\lambda_f - 136606\lambda_f^2 \quad (10)$$

$$\eta_2(\lambda_f) = 109657.3 + 89963.02\lambda_f - 39147.1\lambda_f^2 \quad (11)$$

By substituting Equations (3)~(7) into Equation (2), the creep equation of fiber-reinforced asphalt composite concrete characterized by the Burgers model considering the influence of fiber amount characteristic parameters can be obtained:

Loading stage:

$$\varepsilon(t, \lambda_f) = \sigma_0 \left[\frac{t_0}{\eta_1(\lambda_f)} + \frac{(1 - e^{-t_0\tau})e^{-(t-t_0)}}{E_2(\lambda_f)} \right] \quad (12)$$

The derivative Equation (13) can be used to generate the differential constitutive equation of fiber-reinforced asphalt composite concrete described by the Burgers model taking into account the influence of fiber amount characteristic parameters over time:

Unloading stage:

$$d\varepsilon(t, \lambda_f)/dt = \dot{\varepsilon}(t, \lambda_f) = \sigma_0 \left[\frac{(e^{-t_0\tau} - 1)e^{-(t-t_0)}}{\eta_2(\lambda_f)} \right] \quad (13)$$

4. Discussion

The relationship between the creep strain at the loading stage and the characteristic parameters of fiber amount obtained from Equation (7) is shown in Figure 4. As can be observed, the creep strain drops first and then increases with the increase in fiber amount characteristic parameters, regardless of the same loading time, different stress levels, or the same loading stress, with different loading times. The lowest value is attained when the fiber amount characteristic parameter is around 1.68. The fiber-reinforced asphalt composite concrete now exhibits good resistance to creep deformation. The creep strain of fiber-reinforced asphalt composite concrete increases with increasing tension and loading duration.

Figure 5 depicts the link between the creep rate during the loading stage and the characteristic fiber amount values determined from Equation (8). The smallest value of the creep rate is reached when the fiber amount characteristic parameter is 1.68; the higher the stress, the higher the creep rate. As can be seen, the creep rate first reduces and then increases as the fiber amount characteristic parameter increases. Additionally, Equation (8) demonstrates that as loading time increases, the creep rate decreases.

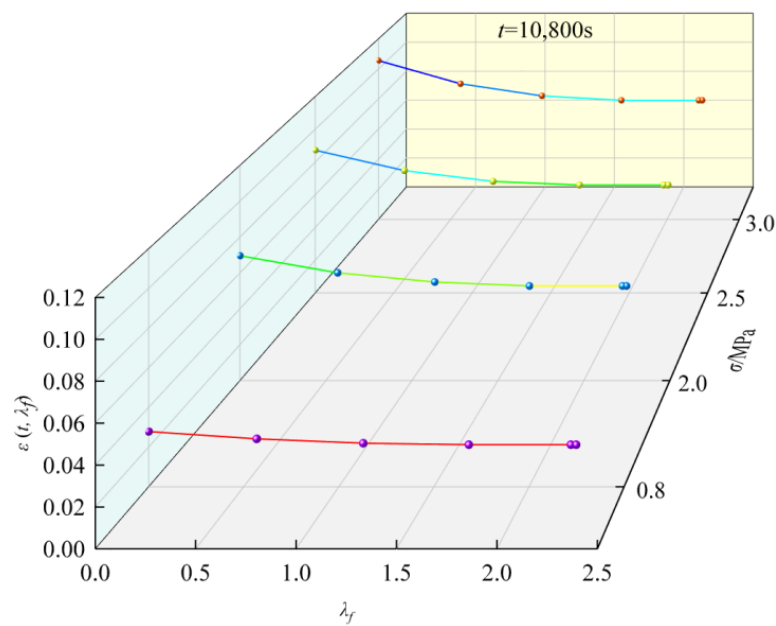


Figure 4. Relationship between creep strain and λ_f .

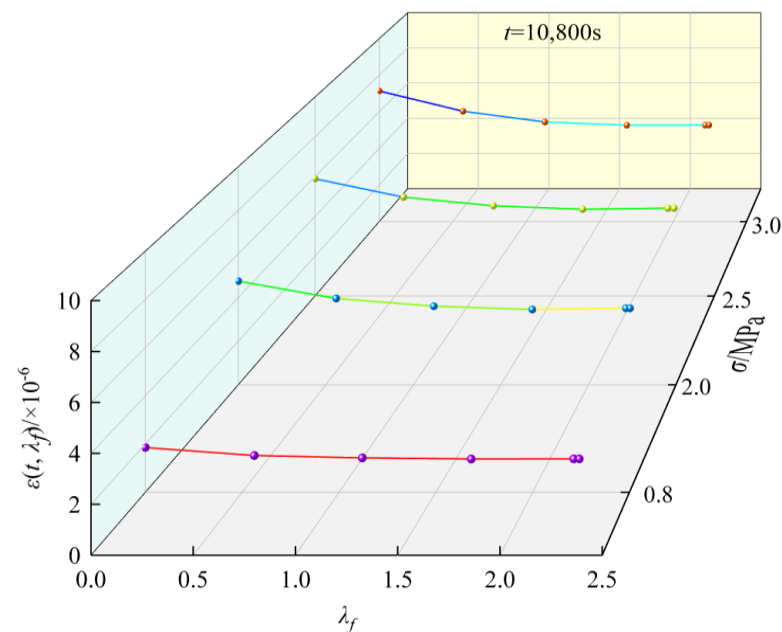


Figure 5. Relationship between creep rate and λ_f .

The relationship between the creep strain of fiber-reinforced asphalt composite concrete after unloading and the characteristic parameters of fiber amount obtained from Equation (12) is shown in Figure 6. It is evident that the residual creep deformation following unloading increases with increasing loading tension. As the characteristic parameter for fiber amount increases, the residual creep deformation first drops and subsequently increases. The minimal residual creep deformation of fiber-reinforced asphalt composite concrete has a fiber amount characteristic parameter value of around 1.13 for the same loading and unloading period and varied loading stress circumstances. Currently, fiber-reinforced asphalt composite concrete has a superior capacity for self-healing creep deformation. Additionally, Equation (12) demonstrates that damage to the fiber-reinforced asphalt composite concrete material and residual creep deformation after unloading increase with the length of the creep loading time.

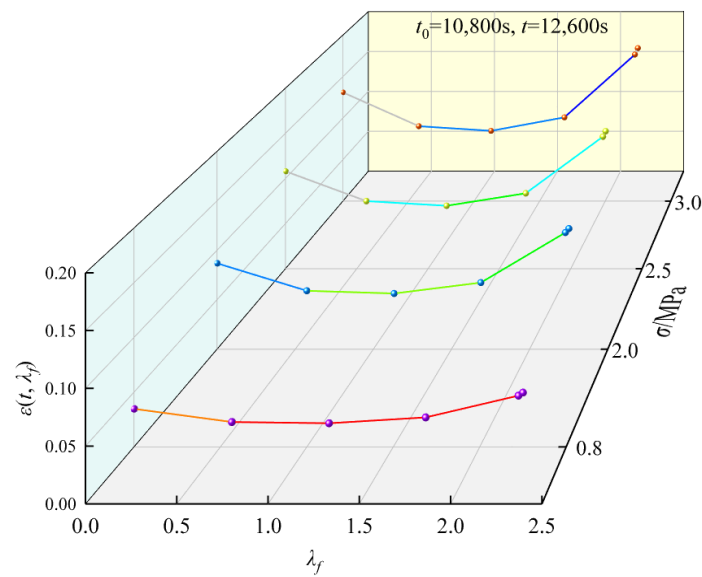


Figure 6. Relationship between creep strain and λ_f .

Figure 7 depicts the link between the fiber-reinforced asphalt composite concrete's post-unloading creep rate and the typical fiber amount characteristics derived from Equation (13). As can be seen, the greater the loading stress, the faster the creep deformation recovers due to the inertia of the immediate recovery of elastic deformation after unloading. With an increase in fiber amount characteristic characteristics, the creep deformation recovery rate first rises and subsequently falls. When the creep deformation recovery rate is at its highest, the fiber amount characteristic characteristics of fiber-reinforced asphalt composite concrete are around 1.13 under the same loading and unloading times and under various loading stress circumstances. Currently, fiber-reinforced asphalt composite concrete has a good capacity for self-healing deformation. Additionally, according to Equation (13), creep load damage to fiber-reinforced asphalt composite concrete increases with loading time and decreases with creep deformation recovery rate.

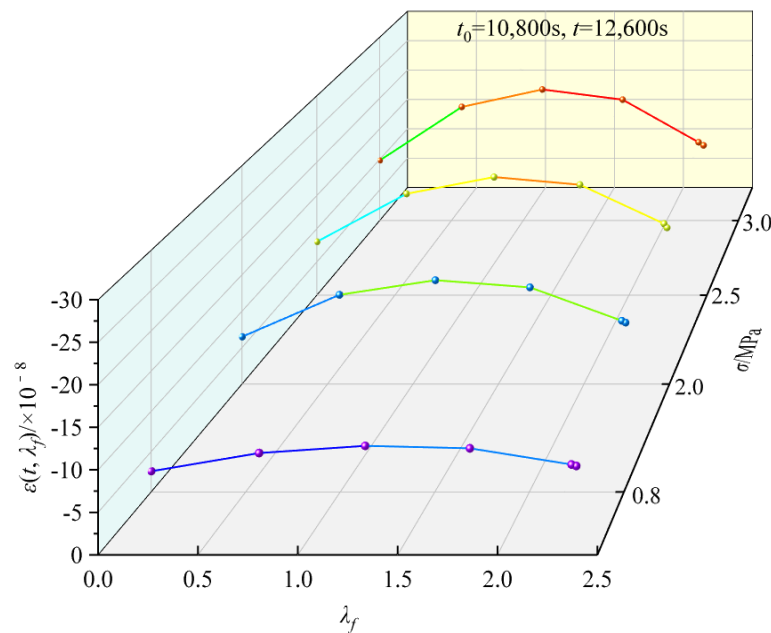


Figure 7. Relationship between creep rate and λ_f .

5. Conclusions and Limitations

Based on the creep test of polyester fiber-reinforced asphalt composite concrete, this paper draws the following conclusions.

According to the results of the fiber-reinforced asphalt composite concrete's creep tests, the position of the creep deformation time relationship curve, the creep rate, the position of the creep compliance time curve, and the instantaneous modulus of resilience following unloading are all lowest when the fiber-volume-fraction is 0.35 percent and the length–diameter-ratio is 324. Currently, fiber-reinforced asphalt composite concrete has strong resilience to elastic deformation after unloading as well as good resistance to creep deformation.

The Burgers model has a strong connection with the test results of fiber-reinforced asphalt composite concrete during the creep loading and unloading stages. This model has a flaw in that it describes the permanent deformation of asphalt composite concrete as a linear function that is inversely related to viscosity and proportionate to time. The model is still unable to accurately depict the deformation characteristics of asphalt composite concrete during the whole loading and unloading operation due to the relationship between viscosity and the increment of permanent deformation.

With an increase in the fiber-volume-fraction and length–diameter-ratio, the model parameters of the Burgers model in the creep loading stage and unloading stage change according to a predetermined pattern. Fiber-reinforced asphalt composite concrete offers superior resistance to elastic deformation, viscous flow deformation, and rutting deformation when the fiber-volume-fraction is 0.35 and the length–diameter-ratio is 324.

The material performance of fiber-reinforced asphalt composite concrete is harmed by creep loading damage. The numerical values of the identical model parameters in the creep loading stage and the creep unloading stage change significantly in the viscoelastic model that represents the creep deformation properties of fiber-reinforced asphalt composite concrete. The deformation features of the unloading process can be more accurately reflected by the Burgers model.

The distinctive fiber amount metrics can fully capture the impact of fiber-volume-fraction and aspect ratio. Burgers model's description of the differential constitutive equation of fiber-reinforced asphalt composite concrete under creep loading, which accounts for the influence of fiber amount's characteristic parameters, may be described by Equation (8). Equation (13) can be used to define the differential constitutive equations of fiber-reinforced asphalt composite concrete in the creep unloading stage as described by the Burgers model while taking the influence of fiber amount characteristic factors into consideration. Theoretical investigation demonstrates that polyester fiber-reinforced asphalt composite concrete has greater deformation resistance and deformation self-healing ability when the characteristic parameter value of polyester fiber amount is 1.13.

In this paper, the applicability of the conclusions drawn from polyester fiber asphalt composite concrete to other types of soft fiber asphalt concrete needs further study. The relationship between the macroscopic mechanical properties and the microstructure of fiber-reinforced asphalt concrete deserves further study. The influence of fiber type and cooling rate on TSRST test parameters of fiber asphalt concrete still needs further study.

Author Contributions: Conceptualization, C.H., D.G. and T.M.; formal analysis, C.H. and C.Y.; investigation, C.H., D.G. and T.M.; methodology, C.H. and D.G.; project administration, C.Y.; supervision, C.Y. All authors have read and agreed to the published version of the manuscript.

Funding: The project was supported by the Key Scientific Research Project of Colleges and Universities in Henan Province (CN) under Grant No. 20A580006, and Horizontal scientific research project of Xuchang University under Grant No. 2022HX006, and the National Natural Science Foundation of China under Grant No. 50678159.

Data Availability Statement: Not applicable.

Conflicts of Interest: The authors declare that they have no conflict of interest.

References

1. Liu, W.; Chen, J.; Luo, Y.; Chen, L.; Shi, Z.; Wu, Y. Deformation behaviors and mechanical mechanisms of double primary linings for large-span tunnels in squeezing rock: A case study. *Rock Mech. Rock Eng.* **2021**, *54*, 2291–2310. [\[CrossRef\]](#)
2. Yuan, B.; Chen, W.; Zhao, J.; Li, L.; Liu, F.; Guo, Y.; Zhang, B. Addition of alkaline solutions and fibers for the reinforcement of kaolinite-containing granite residual soil. *Appl. Clay Sci.* **2022**, *228*, 106644. [\[CrossRef\]](#)
3. Yang, B.; Yuan, S.; Shen, Z.; Zhao, X. Influence of geotextile materials on the fractal characteristics of desiccation cracking of soil. *Fractal Fract.* **2022**, *6*, 628. [\[CrossRef\]](#)
4. Liang, B.; Lan, F.; Shi, K.; Qian, G.; Liu, Z.; Zheng, J. Review on the self-healing of asphalt materials: Mechanism, affecting factors, assessments and improvements. *Constr. Build. Mater.* **2021**, *266*, 120453. [\[CrossRef\]](#)
5. Wang, L.; Huang, Y.; Zhao, F.; Huo, T.; Chen, E.; Tang, S. Comparison between the influence of finely ground phosphorous slag and fly ash on frost resistance, pore structures and fractal features of hydraulic concrete. *Fractal Fract.* **2022**, *6*, 598. [\[CrossRef\]](#)
6. Kassomenos, P.; Vogiatzis, K.; Luis Bento Coelho, J. Critical issues on environmental noise: Editorial. *Sci. Total Environ.* **2014**, *482*, 399. [\[CrossRef\]](#) [\[PubMed\]](#)
7. Darabi, M.; Abu Al-Rub, R.; Masad, E.; Chien-Wei, H.; Little, D. A thermo-viscoelastic-viscoplastic-viscodamage constitutive model for asphaltic materials. *Int. J. Solids Struct.* **2011**, *48*, 191–207. [\[CrossRef\]](#)
8. Zhu, H.; Sun, L. A viscoelastic-viscoplastic damage constitutive model for asphalt mixtures based on thermodynamics. *Int. J. Plast.* **2013**, *40*, 81–100. [\[CrossRef\]](#)
9. Pszczola, M.; Jaczewski, M.; Rys, D.; Jaskula, P.; Szydlowski, C. Evaluation of asphalt mixture low-temperature performance in bending beam creep test. *Materials* **2018**, *11*, 100. [\[CrossRef\]](#)
10. Pucci, T.; Dumont, A.-G.; Di Benedetto, H. Thermomechanical and mechanical behaviour of asphalt mixtures at cold temperature: Road and laboratory investigations. *Road Mater. Pavement* **2004**, *5*, 45–72. [\[CrossRef\]](#)
11. Judycki, J. A new viscoelastic method of calculation of low-temperature thermal stresses in asphalt layers of pavements. *Int. J. Pavement Eng.* **2016**, *19*, 24–36. [\[CrossRef\]](#)
12. Ho, C.-H.; González, M.F.M.; Linares, C.P.M. Effect of asphalt thin beams mixed with three nominal maximum aggregate sizes in the bending beam rheometer on the prediction of thermal properties of bituminous material. *Front. Struct. Civ. Eng.* **2017**, *11*, 1–7. [\[CrossRef\]](#)
13. Park, S.; Kim, Y. Fitting prony-series viscoelastic models with powerlaw presmoothing. *J. Mater. Civ. Eng.* **2001**, *13*, 26–32. [\[CrossRef\]](#)
14. Ho, C.-H.; Romero, P. Using asphalt mixture beams in the bending beam rheometer. Experimental and numerical approach. *Road Mater. Pavement* **2011**, *12*, 293–314. [\[CrossRef\]](#)
15. Tarefder, R.; Faisal, H.; Barlas, G. Freeze-thaw effects on fatigue LIFE of hot mix asphalt and creep stiffness of asphalt binder. *Cold Reg. Sci. Technol.* **2018**, *153*, 197–204. [\[CrossRef\]](#)
16. Huang, W.; Guo, W.; Wei, Y. Thermal effect on rheological properties of epoxy asphalt mixture and stress prediction for bridge deck paving. *J. Mater. Civ. Eng.* **2019**, *31*, 04019222. [\[CrossRef\]](#)
17. Yuan, S.; Sun, B.; Han, G.; Duan, W.; Wang, Z. Application and prospect of curtain grouting technology in mine water safety management in China: A review. *Water* **2022**, *14*, 4093. [\[CrossRef\]](#)
18. Huang, W.; Wang, H.; Yin, Y.; Zhang, X.; Yuan, J. Microstructural modeling of rheological mechanica response for asphalt mixture using an image-based finite element approach. *Materials* **2019**, *12*, 2041. [\[CrossRef\]](#)
19. Gao, D.; Huang, C. Viscoelastic mechanical behavior model with five units and eight parameters for fiber reinforced asphalt composite concrete. *China J. Highw. Transp.* **2014**, *27*, 1–8.
20. Liang, C.; Zhang, H.; Gu, Z.; Xu, X.; Hao, J. Study on mechanical and viscoelastic properties of asphalt mixture modified by diatomite and crumb rubber particles. *Appl. Sci.* **2020**, *10*, 8748. [\[CrossRef\]](#)
21. Yang, B.; Li, D.; Yuan, S.; Jin, L. Role of biochar from corn straw in influencing crack propagation and evaporation in sodic soils. *Catena* **2021**, *204*, 105457. [\[CrossRef\]](#)
22. Ni, B. Mechanical Response Analysis of Viscoelastic Layered System in Asphalt Pavement. Master's Thesis, Dalian University of Technology, Dalian, China, 2014.
23. Yuan, S.; Yang, B.; Liu, J.; Cao, B. Influence of fibers on desiccation cracks in sodic soil. *Bull. Eng. Geol. Environ.* **2021**, *80*, 3207–3216. [\[CrossRef\]](#)
24. Lundstroem, R.; Isacson, U. Linear viscoelastic and fatigue characteristics of styrene-butadiene-styrene modified asphalt mixtures. *J. Mater Civ. Eng.* **2004**, *166*, 629–638. [\[CrossRef\]](#)
25. Polacco, G.; Stastna, J.; Biondi, D.; Zanzotto, L. Relation between polymer architecture and nonlinear viscoelastic behavior of modified asphalts. *Curr. Opin. Colloid In.* **2006**, *11*, 230–245. [\[CrossRef\]](#)
26. Judycki, J. Non-linear viscoelastic behaviour of conventional and modified asphalt composite concrete under creep. *Mater. Struct.* **1992**, *25*, 95–101. [\[CrossRef\]](#)
27. Yuan, S.; Han, G. Combined drilling methods to install grout curtains in a deep underground mine: A case study in Southwest China. *Mine Water Environ.* **2020**, *39*, 902–909. [\[CrossRef\]](#)
28. Guo, N.; Zhao, Y. Viscoelastic performance analysis of fiber reinforced asphalt composite concrete. *J. Traffic Transp. Eng.* **2007**, *10*, 37–40. (In Chinese with abstract in English)

29. Feng, J. Study of Performance and Mechanism of Fiber Reinforced Asphalt Mixtures. Ph.D. Thesis, Southeast University, Nanjing, China, 2007.
30. Chen, J.S.; Lin, K.Y. Mechanism and behavior of bitumen strength reinforcement using fibers. *J. Mater. Sci.* **2005**, *40*, 87–95. [[CrossRef](#)]
31. Bueno, B.D.; da Silva, W.R.; de Lima, D.C.; Minete, E. Engineering properties of fiber reinforced cold asphalt mixes. *J. Environ. Eng.* **2003**, *129*, 952–955. [[CrossRef](#)]
32. Chen, H.X. Study on Fiber Asphalt Composite Concrete Pavement. Master's Thesis, Chang'an University, Xi'an, China, 2002.
33. Zhou, Z.G. A Research on the Fatigue Damage Cracking in Asphalt Pavement under Traffic Load. Ph.D. Thesis, Central South University, Changsha, China, 2003.
34. Chen, Z.N. Asphalt Adsorption Mechanism of Corn Stalk Fiber and Road Performance Research of Corn Stalk Fiber SMA. Ph.D. Thesis, Harbin Industrial University, Harbin, China, 2021.
35. Yuan, B.; Li, Z.; Chen, W.; Zhao, J.; Lv, J.; Song, J.; Cao, X. Influence of groundwater depth on pile-soil mechanical properties and fractal characteristics under cyclic loading. *Fractal Fract.* **2022**, *6*, 198. [[CrossRef](#)]
36. Yuan, B.; Chen, M.; Chen, W.; Luo, Q.; Li, H. Effect of pile-soil relative stiffness on deformation characteristics of the laterally loaded pile. *Adv. Mater. Sci. Eng.* **2022**, *2022*, 4913887. [[CrossRef](#)]
37. Yuan, B.; Chen, W.; Zhao, J.; Yang, F.; Luo, Q.; Chen, T. The effect of organic and inorganic modifiers on the physical properties of granite residual soil. *Adv. Mater. Sci. Eng.* **2022**, *2022*, 9542258. [[CrossRef](#)]
38. Xu, B.; Blok, R.; Teuffel, P. An investigation of the effect of relative humidity on viscoelastic properties of flax fiber reinforced polymer by fractional-order viscoelastic model. *Compos. Commun.* **2023**, *37*, 101406. [[CrossRef](#)]
39. Al-Sakkaf, A.; Bagchi, A.; Zayed, T.; Mahmoud, S. Sustainability assessment model for heritage buildings. *Smart Sustain. Built.* **2023**, *12*, 105–127. [[CrossRef](#)]
40. Wang, L.; Zhou, S.; Shi, Y.; Huang, Y.; Zhao, F.; Huo, T.; Tang, S. The influence of fly ash dosages on the permeability, pore structure and fractal features of face slab concrete. *Fractal Fract.* **2022**, *6*, 476. [[CrossRef](#)]
41. Russo, F.; Veropalumbo, R.; Oreto, C. Climate change mitigation investigating asphalt pavement solutions made up of plastomeric compounds. *Resour. Conserv. Recy.* **2023**, *189*, 106772. [[CrossRef](#)]

Disclaimer/Publisher's Note: The statements, opinions and data contained in all publications are solely those of the individual author(s) and contributor(s) and not of MDPI and/or the editor(s). MDPI and/or the editor(s) disclaim responsibility for any injury to people or property resulting from any ideas, methods, instructions or products referred to in the content.